Engineering Structures 33 (2011) 3432–3441

Contents lists available at SciVerse ScienceDirect

Engineering Structures

journal homepage: www.elsevier.com/locate/engstruct

Upper and lower bounds for structural design of RC members with ductile response

A. Carpinteri, M. Corrado *

Politecnico di Torino, Department of Structural Engineering and Geotechnics, Corso Duca degli Abruzzi 24, 10129, Torino, Italy

ARTICLE INFO

Article history:
Received 27 January 2011
Received in revised form
1 June 2011
Accepted 1 July 2011
Available online 4 August 2011

Keywords:
Reinforced concrete
Rotational capacity
Minimum reinforcement
Size effects
Fracture mechanics
Dimensional analysis
Code provisions

ABSTRACT

In the present paper, some of the complex phenomena characterizing the flexural behaviour of reinforced concrete beams, such as hyper-strength and snap-back and snap-through instabilities, are interpreted under a unified approach based on nonlinear fracture mechanics concepts. In particular, they are analysed by means of a numerical algorithm adopting the *cohesive crack model* for concrete in tension and the *overlapping crack model* for concrete in compression. According to the latter constitutive law, a fictitious interpenetration is assumed to describe the concrete damage, analogously to the fictitious crack opening used for tension.

Such an integrated cohesive-overlapping crack model is applied to assess the minimum reinforcement amount necessary to prevent unstable tensile crack propagation and to evaluate the rotational capacity of plastic hinges. The main novelty is given by the capability to predict the size-scale effects evidenced by several experimental programmes available in the literature. According to the numerical results obtained, new practical design formulae and diagrams are proposed, as well as, upper and lower bounds to the reinforcement amount, the material properties and the structural dimensions are defined in order to avoid brittle failures.

1. Introduction

The global response of reinforced concrete (RC) beams in bending during the loading process is characterized by complex phenomena due to mechanical nonlinearities, as evidenced in the qualitative moment vs. rotation diagram shown in Fig. 1. In more details, we refer to concrete fracturing, which produces a hyper-strength in the increasing branch, steel yielding, which is at the origin of a ductile behaviour, and concrete crushing, which determines a decrease in the load carrying capacity and, consequently, a limit to the ultimate rotation.

Although two failure modes are usually observed in the flexural behaviour, i.e., yielding of the steel reinforcement and crushing of the compressed concrete, more complex phenomena can affect the load vs. displacement relationships: snap-through instability, defined as a loss of stability in the controlled load condition, and snap-back instability, representing a loss of stability in the controlled displacement condition. Such phenomena are very general, and usually encountered in structural problems characterized by either geometrical or mechanical nonlinearities. As an example, they may appear in the buckling response of elastic structures, as evidenced by von Kármán and Tsien [1] for thin cylindrical shells under axial compression, and by Carlson et al. [2] and Kaplan [3] for complete spherical shells and spherical caps subjected to external pressure. On the other hand, snap-back instabilities can be easily encountered when materials exhibiting strain softening behaviours are considered. This is, for instance, the case of plain concrete slabs in tension and in bending, whose overall responses are highly influenced by the softening behaviour of the process zone ahead of the real crack tip. The detailed analytical and numerical investigations carried out by Carpinteri [4,5] by means of the *cohesive crack model* put into evidence a transition from softening to snap-back instability either by increasing the specimen dimensions and/or the material strength, or by decreasing the material fracture energy. The virtual post-peak catastrophic branch, characterized by a positive slope in the load vs. displacement plane, can be captured only if the loading process is controlled by the crack mouth opening displacement. In this context, the application of the cohesive crack model to three-point-bending tests on plain concrete beams has permitted to describe the size effects on the nominal flexural tensile strength, σ_n, function of the maximum load in the hypotheses of linear strain distribution along the cross-section and linear-elastic behaviour for concrete in tension and compression. The numerical results, as a function of the beam height, are compared to the empirical prescriptions provided by the Model Code 90 [6] and the Eurocode 2 [7] in Fig. 2. The ratio σ_n/σ_u, where σ_u is the limit stress that the material can locally sustain and, therefore, is a material property, tends to unity only for very large heights, h,

* Corresponding author. Tel.: +39 011 5644873; fax: +39 011 5644899.
E-mail address: mauro.corrado@polito.it (M. Corrado).

0141-0296/$ – see front matter © 2011 Elsevier Ltd. All rights reserved.
doi:10.1016/j.engstruct.2011.07.007

Notations

A_s	Steel reinforcement area;
b	Thickness of the beam;
d	Effective depth of the beam;
D_M	Coefficient of influence for the applied moment;
$\{D_w\}^T$	Vector of the coefficients of influence for the nodal displacements;
E_c	Elastic modulus of concrete;
$\{F\}$	Vector of nodal forces;
$\mathcal{G}_C$	Crushing energy of concrete;
$\mathcal{G}_F$	Fracture energy of concrete;
$\{K_M\}$	Vector of the coefficients of influence for the applied moment;
K_w	Matrix of the coefficients of influence for the nodal displacements;
h	Overall beam height;
L	Span of the beam;
l	Length of the considered beam element;
M	Applied bending moment;
N_C	Stress brittleness number in compression;
N_P^L	Lower limit for the reinforcement brittleness number;
N_P^U	Upper limit for the reinforcement brittleness number;
P	Applied load;
s	Stress brittleness number in tension;
$\{w\}$	Vector of nodal displacements;
w_{cr}^c	Critical overlapping displacement;
w_{cr}^t	Critical crack opening displacement;
δ	Mid-span deflection;
$\varepsilon_{c,u}$	Ultimate elastic compressive strain of concrete;
$\varepsilon_{t,u}$	Ultimate elastic tensile strain of concrete;
ϑ	Localized rotation of the considered beam element;
ϑ_{PL}	Plastic component of the localized rotation;
ρ	$(A_s/bh) \times 100$, steel reinforcement percentage;
σ_c	Average compressive strength of concrete;
σ_n	Nominal flexural tensile strength of concrete;
σ_u	Average tensile strength of concrete;
σ_y	Tensile yield strength of steel.

whereas it is equal to three for h tending to zero. Such an increase in the apparent tensile strength is due to the combined effect of the post-peak softening behaviour and the high strain gradient characterizing the bending condition.

Transitions from softening to snap-back instability also characterize the overall response of quasi-brittle materials in compression by varying the specimen size and/or slenderness (see the experimental tests by van Mier [8] and Jansen and Shah [9]). In this context, recent analytical and numerical studies have been carried out by Carpinteri et al. [10,11] in the case of concrete specimens subjected to uniaxial and eccentric compression.

Finally, snap-through local instabilities are often evidenced in the case of composite materials, such as reinforced and fibre-reinforced concrete, due to the fact that fibres act as crack-arrest mechanisms, producing a global ductile response. Experimental evidence has been found in cement matrix specimens reinforced by glass-fibre bundles [12], reinforced concrete beams [13], and alumina matrix samples with SiC whiskers [14]. Very interesting interpretations of such phenomenon have been proposed by means of the *bridged crack model* [15–17].

All the aforementioned aspects hold a fundamental role in the study of RC members, where the application of simplified constitutive relations for concrete do not permit to model all

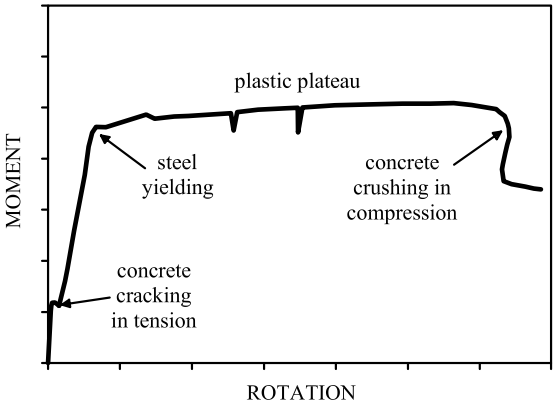

Fig. 1. Nonlinear contributions involved in the flexural behaviour of RC elements.

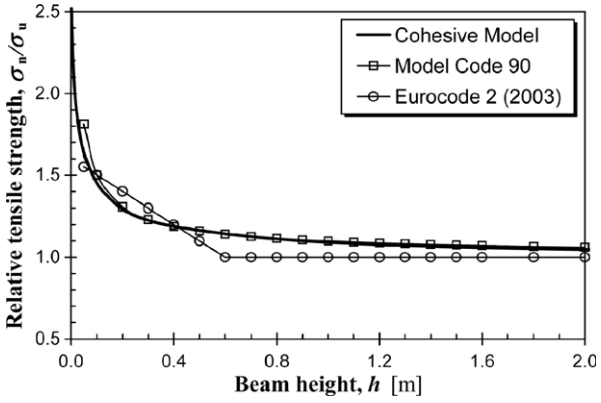

Fig. 2. Size-effect on the flexural tensile strength: application of the cohesive crack model and prescriptions of the design codes.

the experimentally observed effects. In the stress–strain laws proposed by Standards, in fact, the concrete tensile contribution as well as the softening branch and the localization of strain in the post-peak regime both for tension and compression, are usually neglected. In the case of low reinforcement percentages, for instance, the tensile concrete contribution, may determine a hyper-strength with respect to the ultimate loading condition, and a consequent possible instability in the overall mechanical response, the post-peak cracking moment being a monotonic decreasing function of the crack length. For this reason, all national and international codes of practice provide empirical formulae for the determination of the minimum reinforcement amount which enable RC members to prevent unstable crack propagation. To this regard, it is worth noting that most of these prescriptions do not consider the size effects. Analogously, the most common approaches used to analyse the behaviour of over-reinforced concrete beams in bending, usually based on stress vs. strain constitutive laws for concrete in compression, do not permit to describe the decrease in the load carrying capacity due to concrete crushing and the experimentally observed size effects on the plastic rotation capacity [18–20]. It has to be noticed that, also in this case, the current prescriptions provided by codes of practice completely disregard the effects of the member size.

In the present paper, the main features of a numerical method recently developed by Carpinteri et al. [21,22] able to describe the nonlinear behaviour of RC members during both fracturing and crushing is briefly outlined. In particular, it will be shown that the crushing process can be efficiently analysed according to the *overlapping crack model* [10], which considers a fictitious material interpenetration in the post-peak regime. With the proposed algorithm it is possible to completely capture the moment vs. rotation response of several experimental tests available in the literature. As a

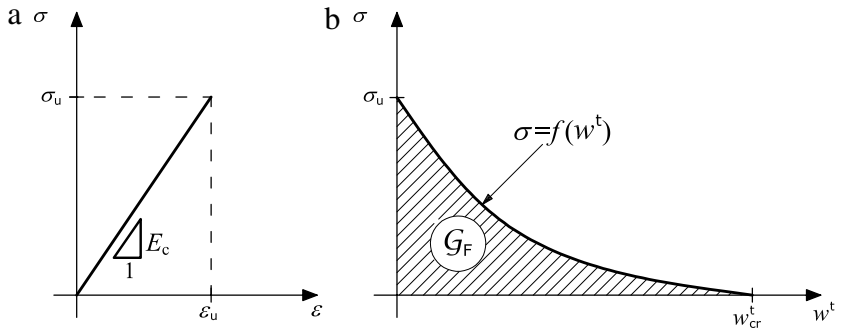

Fig. 3. Cohesive crack model: (a) linear-elastic $\sigma-\varepsilon$ law; (b) post-peak softening $\sigma-w$ relationship.

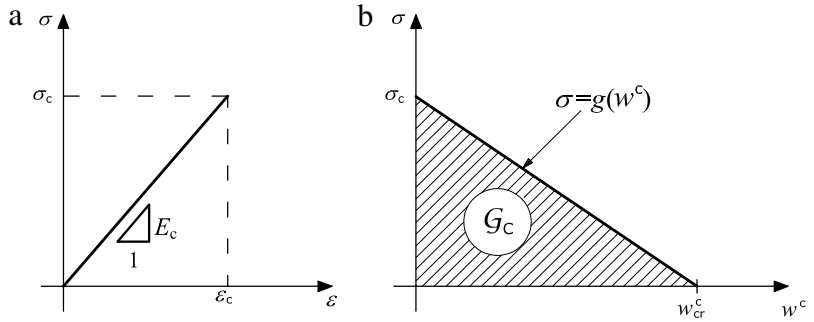

Fig. 4. Overlapping crack model: (a) linear-elastic $\sigma-\varepsilon$ law; (b) post-peak softening $\sigma-w$ relationship.

result of a parametric investigation, a new relationship for the minimum reinforcement amount, which is affected by size-scale effects, will be determined. It will be shown that the prescriptions of some codes are not conservative for small structural sizes, whereas other ones over-estimate the minimum amount, especially in the case of large structural sizes. Then, plastic rotation vs. neutral axis position curves will be determined, that are found to be dependent on the structural dimension and the steel percentage. Also in this case, it will be shown that the European prescriptions do not consider the transition from ductile-to-brittle response by increasing the structural size, leading to over-estimate the rotational capacity of large beams.

2. Numerical approach

In this section, the numerical algorithm proposed by Carpinteri et al. [21,22] for the analysis of the mechanical behaviour of a portion of an RC beam subjected to a constant bending moment, M, is briefly described. This element, having a span to height ratio equal to unity, is representative of the zone of a beam where a plastic hinge formation takes place. Such a ratio has been chosen according to the experimental evidence that most of the contributions to the plastic rotation are generated within this portion (as an example, the Eurocode 2 [7] suggests to consider a ratio equal to 1.2). Then, it is assumed that fracturing and crushing processes are fully localized along the mid-span cross-section of the element, whereas the part of the hinge outside the localization zone is assumed elastic. This assumption also implies that only one equivalent main tensile crack is considered. The loading process is characterized by crack propagation in tension, steel yielding and/or slippage as well as concrete crushing in compression.

2.1. Constitutive models

In the proposed algorithm, the behaviour of concrete in tension is described by means of the well established cohesive crack model [23], largely used, in the past, to study the ductile-to-brittle transition in plain concrete beams in bending [5]. According to this model, the adopted constitutive law is a stress–strain linear-elastic relationship up to the achievement of the average tensile strength, σ_u, for the undamaged zone (Fig. 3(a)), and a stress–displacement relationship describing the process zone behaviour up to the critical opening, w_{cr}^t, beyond which the transferred traction vanishes (Fig. 3(b)). The softening function, $\sigma = f(w)$, is considered as a material property, as well as the critical value of the crack opening, w_{cr}^t, and the fracture energy, $\mathcal{G}_F$. The shape of $f(w)$ may vary from linear to bilinear or even more complicated relationships depending on the characteristics of the material considered and the problem analysed. The critical value of the crack opening displacement is approximately equal to 0.1 mm, and the fracture energy is assumed to vary from 0.050 N/mm to 0.150 N/mm, depending on concrete strength and maximum aggregate diameter, according to the prescriptions given by the Model Code 90.

As far as modelling of concrete crushing failure is concerned, the overlapping crack model [10] is adopted. According to such an approach, based on the original insights provided by Kotsovos [24] and van Mier [8], and related to the pioneering work by Hillerborg [25], the inelastic and localized deformation in the post-peak regime is described by a fictitious interpenetration of the material, while the remaining part of the specimen undergoes an elastic unloading. As a result, a pair of constitutive laws for concrete in compression is introduced, in close analogy with the cohesive crack model: a stress–strain relationship until the compressive strength is achieved (Fig. 4(a)), and a stress–displacement (overlapping) relationship describing the phenomenon of concrete crushing (Fig. 4(b)). The latter law, approximated by a linear softening relationship for modelling purposes, describes how the stress in the damaged material decreases from its maximum value as the fictitious interpenetration increases. It is worth noting that the crushing energy, $\mathcal{G}_C$, which is a dissipated surface energy, is defined as the area below the post-peak softening curve in Fig. 4(b). It can be assumed as a true material property, since it is only slightly affected by the structural size, as shown in Ref. [11], where a large validation of the overlapping model for concrete-like materials has

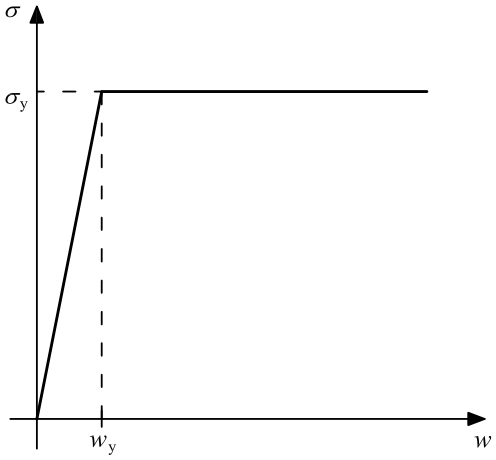

Fig. 5. Elasto-plastic $\sigma-w$ constitutive law for steel rebars.

been proposed in the case of specimens with different values of slenderness and/or sizes. Certainly, it is worth noting that the compressive damage is a more spread phenomenon, characterized by an energy dissipation within multiscale or fractal domain. On the other hand, the value of the physical dimension of such domains, closer to 2.0 than 3.0 (about 2.3 for concrete, according to the analysis performed by Carpinteri and Corrado [26]), makes clear the effectiveness of the simplified overlapping crack model, which, in fact, assumes a dissipation over a surface. By varying the concrete average compressive strength from 20 to 90 MPa, the crushing energy ranges from 30 to 58 N/mm. The critical value for the crushing interpenetration, w_{cr}^{c}, is experimentally found to be approximately equal to 1 mm, and it is a decreasing function of the compressive strength. When lateral confinement is exerted by stirrups, the empirical equation recently proposed by Suzuki et al. [27] can be applied to calculate the crushing energy. Both $\mathcal{G}_C$ and w_{cr}^{c} are increasing functions of concrete confinement.

As far as the behaviour of the steel reinforcement is concerned, it is impossible to adopt the classical $\sigma-\varepsilon$ laws, since the kinematics of the mid-span cross-section of the RC member is described by means of displacements, instead of strains. Therefore, we assume that the reinforcement acts through concentrated forces, functions of the relative opening displacement, equilibrating the generalized stress torque in the cross-section. To this aim, constitutive relationships between the reinforcement reaction and the crack opening displacement are obtained by means of preliminary studies carried out on the interaction between the reinforcing bar and the surrounding concrete. The integration of the differential slips over the transfer length, l_{tr}, is equal to half the crack opening at the reinforcement level, whereas the integration of the bond stresses gives the reinforcement reaction. Simplified procedures of such an approach have been proposed by Ruiz et al. [28]. Typically, the relationships obtained are characterized by an ascending branch up to steel yielding, to which corresponds the critical value of the crack opening for steel, w_y (see Fig. 5). After that, the steel reaction is nearly constant. As regards the value of w_y, it is affected by the parameters influencing the bond–slip behaviour, such as the diameter, the number and the roughness of the rebars. In this study, an average value equal to 0.3 mm has been used for any steel percentages. It can be assumed as the representative for ribbed bars, commonly used in practical applications. The contribution of the steel yielding strain to w_y is considered as negligible compared to the steel–concrete slip. Due to lack of studies on the behaviour of reinforcing bars in compression, the same $\sigma-w$ relationship is adopted for both tension and compression.

2.2. Numerical algorithm

The RC member is considered as constituted by two symmetrical elements characterized by an elastic behaviour, and connected by means of (n) pairs of nodes (Fig. 6(a)). In this approach, all the mechanical nonlinearities are localized in the mid-span cross-section, where cohesive and overlapping stresses are replaced by equivalent nodal forces, F_i, by integrating the corresponding stresses over the nodal spacing. Such nodal forces depend on the nodal opening or closing displacements according to the cohesive or overlapping softening laws previously introduced.

With reference to Fig. 6(a), the horizontal forces, F_i, acting at the ith node along the mid-span cross-section can be computed as follows:

$$\{F\} = [K_w]\{w\} + \{K_M\}M, \tag{1}$$

where: $\{F\}$ is the vector of nodal forces, $[K_w]$ is the matrix of the coefficients of influence for the nodal displacements, $\{w\}$ is the vector of nodal displacements, $\{K_M\}$ is the vector of the coefficients of influence for the applied moment M.

Eq. (1) constitutes a linear algebraic system of (n) equations and $(2n+1)$ unknowns, $\{F\}$, $\{w\}$ and M. With reference to the generic situation reported in Fig. 6(b), (n) additional equations can be introduced by considering the constitutive laws for concrete in tension and compression and for the reinforcement in the node r (see [22] for more details). The last additional equation derives from the strength criterion adopted to govern the propagation processes. At each step of the loading process, in fact, we can set either the force in the fictitious crack tip, m, equal to the ultimate tensile force, F_u, or the force in the fictitious crushing tip, p, equal to the ultimate compressive force, F_c. It is important to note that the condition for crack propagation (corresponding to the achievement of the tensile strength at the fictitious crack tip, m) does not imply that the compressive strength is reached at the

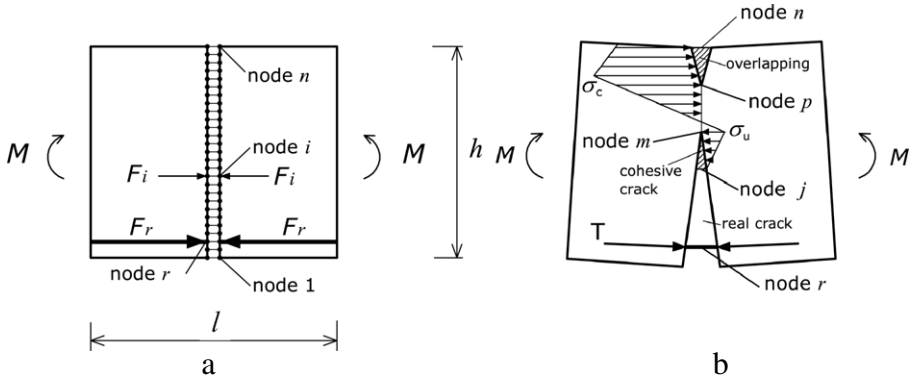

Fig. 6. Finite element nodes (a); and force distribution with cohesive crack in tension and crushing in compression (b) along the mid-span cross-section.

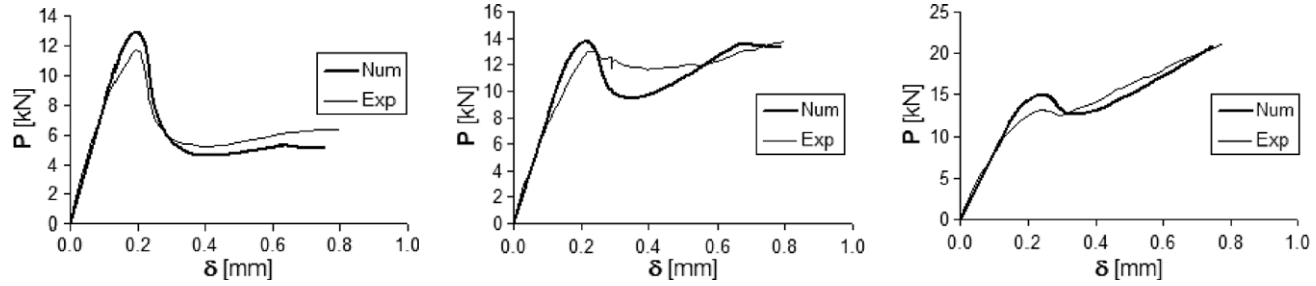

(a) $\rho = 0.085\%$. (b) $\rho = 0.256\%$. (c) $\rho = 0.653\%$.

Fig. 7. Comparison between numerical and experimental [13] load vs. mid-span deflection curves for beam height $h = 0.1$ m.

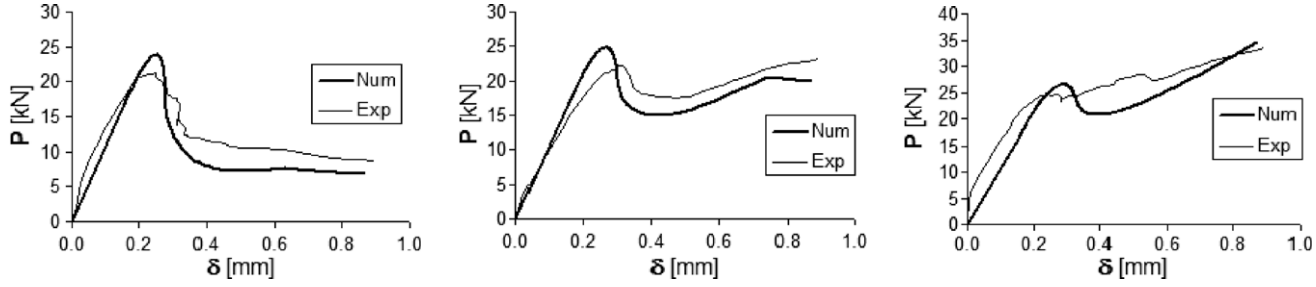

(a) $\rho = 0.064\%$. (b) $\rho = 0.190\%$. (c) $\rho = 0.490\%$.

Fig. 8. Comparison between numerical and experimental [13] load vs. mid-span deflection curves for beam height $h = 0.2$ m.

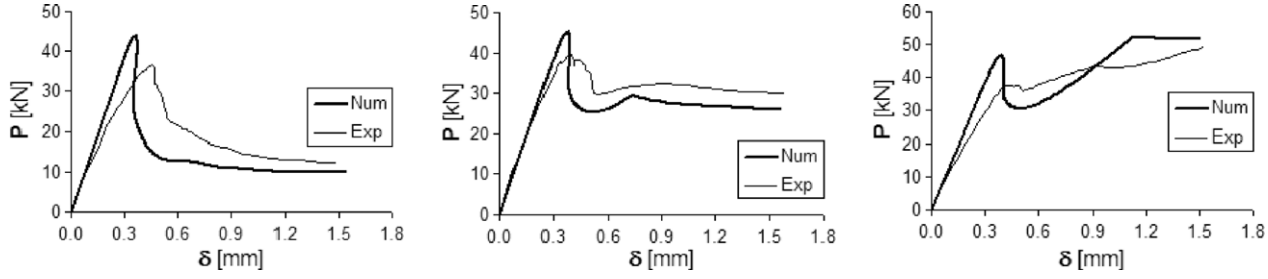

(a) $\rho = 0.043\%$. (b) $\rho = 0.128\%$. (c) $\rho = 0.327\%$.

Fig. 9. Comparison between numerical and experimental [13] load vs. mid-span deflection curves for beam height $h = 0.4$ m.

corresponding overlapping crack tip, p, and *vice versa*. Hence, the driving parameter of the process is the tip that in the considered step has reached the limit resistance. Only this tip is moved when passing to the next step. Finally, at each step of the algorithm, it is possible to calculate the localized beam rotation, ϑ, as follows:

$$\vartheta = \{D_w\}^T\{w\} + D_M M, \tag{2}$$

where $\{D_w\}$ is the vector of the coefficients of influence for the nodal displacements and D_M is the coefficient of influence for the applied moment. It has to be observed that the coefficients entering Eqs. (1) and (2) are computed *a priori* using a linear finite element analysis. They are connected by simple relations of proportionality to the structural dimension, and, therefore, it is not necessary to repeat the finite element analysis for any different considered beam size.

3. Comparison of numerical predictions and experimental results

In this section, a comparison between the numerical predictions using the cohesive/overlapping crack model and the results of two experimental campaigns is presented. First, the three-point-bending tests carried out by Bosco et al. [13] on reinforced high-strength concrete beams to investigate the size-scale effects on the minimum reinforcement amount are considered. Three different size-scales were analysed, characterized by a overall height, h, equal to 0.1, 0.2 and 0.4 m, and a constant width, b, equal to 0.15 m. The span to depth ratio was equal to 6. Five different steel percentages, ρ, were considered for each beam size. The model parameters have been set equal to the actual concrete and steel properties, that can be deduced from Ref. [13]. In the numerical simulations, the RC element of Fig. 6(a) is assumed to be representative of the mid-span portion of the beam subjected to three-point-bending test. As a result, the mid-span deflection is obtained as the sum of the localized rotation given by Eq. (2), and the elastic contribution, according to the following expression:

$$\delta = \delta_{\text{loc}} + \delta_{\text{el}} = \frac{\vartheta L}{4} + \frac{1}{48}\frac{PL^3}{E_c I^*} \tag{3}$$

where L is the beam span, P is the applied load, E_c is the concrete elastic modulus, and I^* is a reduced moment of inertia of the cross-section, introduced to take into account the stiffness reduction due to smeared cracking along the beam span. The hypothesis of localization of the nonlinearities along the symmetry cross-section, in fact, does not permit to consider this effect. More in details, the value of I^* is empirically selected in order to obtain the stiffness of the increasing branch of the numerical load vs. deflection curves equal to the experimental ones (see Figs. 7–9). In the present study, the problem has not been deepened more

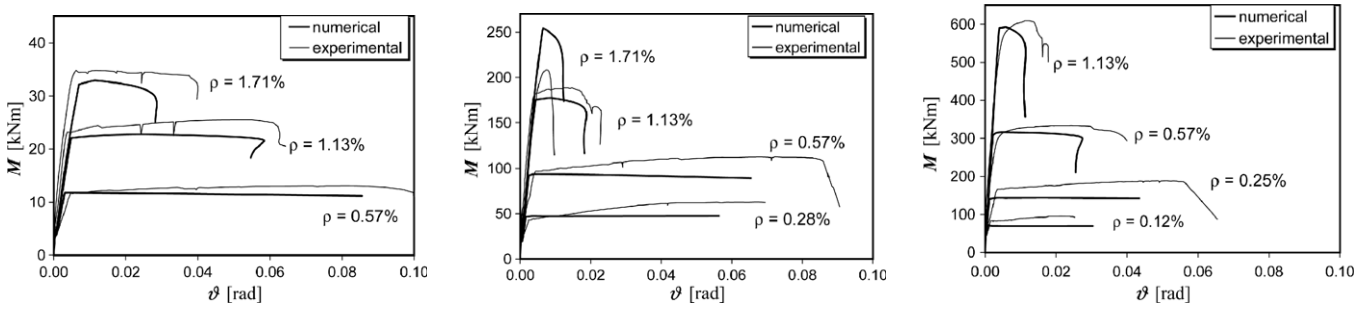

(a) $h = 0.2$ m. (b) $h = 0.4$ m. (c) $h = 0.6$ m.

Fig. 10. Comparison between numerical and experimental results [20] for different beam heights: $h = 0.2$ m (a); $h = 0.4$ m (b); $h = 0.6$ m (c).

since it does not influence the minimum and maximum steel percentages, defined on the basis of load carrying capacities. Some of the numerical simulations compared to the corresponding experimental results, in terms of applied load vs. mid-span deflection curves, are shown in Figs. 7–9. Such curves evidence a transition from an overall softening response to a hardening response by increasing the steel percentage, with the appearance of local snap-through instabilities. Furthermore, it is worth noting that the condition for which the peak-cracking load is equal to the ultimate load occurs for values of reinforcement percentage decreasing with the beam size (curves *b* in Figs. 7–9). Such a phenomenon evidence a size-scale effect.

Aiming at a further validation of the proposed model in the case of high steel percentages, the experimental analysis carried out by Bosco and Debernardi [20] on RC beams to investigate the size-scale effects on the rotational capacity is also considered. In order to obtain a consistent comparison, the numerical simulations have been carried out by modelling the beam portion positioned at the mid-span of the beam. This element is characterized by a span to height ratio equal to one. The rotations of such a portion, where the largest amount of ductility is developed, were experimentally determined as functions of the applied bending moment. Also in this case, the mechanical and geometrical parameters are set equal to the experimental values. Numerical and experimental moment–rotation curves are compared in Fig. 10(a)–(c) for different beam heights and different steel percentages. Such diagrams put into evidence that the maximum rotation is a decreasing function of the tensile reinforcement ratio and of the beam height. In the case of low steel percentages, the mechanical behaviour is characterized by the reinforcement yielding and the mechanical response is almost plastic. By increasing the reinforcement amount, the contribution of concrete crushing becomes more and more evident with the appearance of a softening branch at the end of the plastic plateau. This is an important feature of the proposed model, which also permits to follow snap-back branches by controlling the loading process through the length of the tensile crack and the extension of the fictitious crushing zone, rather than by the external load or the central deflection. Good agreement was obtained between numerical and experimental results for all the tested beams.

4. Numerical results and practical prescriptions for design

4.1. Minimum reinforcement

In this section, a new relationship between the minimum reinforcement and the mechanical and geometrical parameters is proposed on the basis of a wide parametric analysis. To this aim, different values of the beam height, h, ranging from 0.1 and 3.2 m, and different values of the concrete average compressive strength, σ_c, ranging from 16 to 76 MPa, have been considered. All the other mechanical properties of concrete, as, for instance, the tensile strength and the fracture energy, have been evaluated according to the relationships provided by the Model Code 90 [6] and reported in Table 1. As regards the steel reinforcement, a yield strength $\sigma_y = 600$ MPa, and an elastic modulus $E_s = 200$ GPa have been assumed. The ratio between effective and overall depth, d/h, has been fixed equal to 0.9. For each of the considered beams, several simulations have been carried out by varying the steel percentage, in order to find the minimum reinforcement amount. In particular, such a value is determined when the peak cracking load, P_{cr}, is equal to the ultimate load, P_u, as shown in Fig. 11(a).

In order to better clarify the effects of each of the variables involved in the physical phenomenon, as well as their interaction to govern the global response, a reduction of the primary variables is obtained by combining them into dimensionless groups by means of *dimensional analysis*. According to the numerical model proposed in the previous section, the general functional relationship among the quantities that characterize the phenomenon is the following:

$$M = \phi\left(\sigma_u, \mathcal{G}_F, \sigma_c, \mathcal{G}_C, E_c, \sigma_y, \rho, h; \frac{b}{h}, \frac{l}{h}, \vartheta\right). \tag{4}$$

When the flexural behaviour of lightly-reinforced concrete beams is studied, the parameters describing the behaviour of concrete in compression, σ_c and $\mathcal{G}_C$, can be omitted, since the crushing failure is not involved in the failure mechanism. On the other hand, only the beam height, h, can be considered if the geometrical ratios of the samples, b/h and l/h, are assumed to be constant. This assumption permits to investigate the size effects – all the beam dimensions varying with the beam height – whereas the effects of the width and the slenderness are not taken into account. More precisely, the resistant moment is assumed to be independent of the slenderness, and linearly dependent on the beam width.

Under these hypotheses, the application of Buckingham's Π-Theorem [29] for physical similarity and scale modelling yields to the following relationship:

$$\frac{M}{h^{2.5}\sqrt{\mathcal{G}_F E_c}} = \Phi_1\left(\frac{\sigma_u h^{0.5}}{\sqrt{\mathcal{G}_F E_c}}, \rho\frac{\sigma_y h^{0.5}}{\sqrt{\mathcal{G}_F E_c}}, \vartheta\frac{E_c h^{0.5}}{\sqrt{\mathcal{G}_F E_c}}\right), \tag{5}$$

if h and $\sqrt{\mathcal{G}_F E_c}$, which corresponds to the material toughness K_{IC}, are assumed as the dimensionally independent variables. As a consequence, the dimensionless functional relation for the proposed model becomes:

$$\tilde{M} = \Phi_2(s, N_P, \vartheta_n), \tag{6}$$

where:

$$s = \frac{K_{IC}}{\sigma_u h^{0.5}} \tag{7}$$

and

$$N_P = \rho\frac{\sigma_y h^{0.5}}{K_{IC}} \tag{8}$$

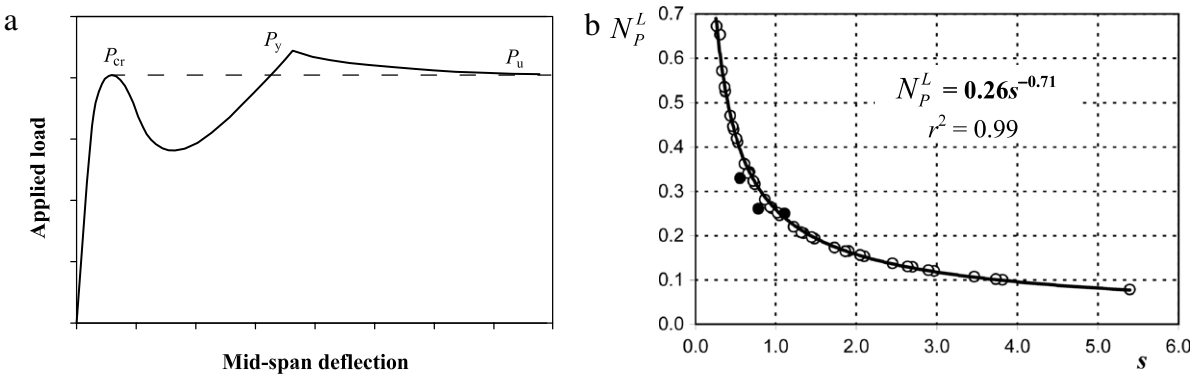

Fig. 11. Definition of minimum reinforcement (a); and best-fit relationship of numerical results (not filled-in symbols) between N_P^L and s. Filled-in symbols refer to the experimental results from [13].

Table 1
Mechanical and geometrical parameters of the beams considered in the numerical simulations.

σ_c (MPa)	σ_u (MPa)	G_F (N/mm)	E_c (MPa)	G_C (N/mm)	h (mm)	$\rho_{\min}$ (%)	s	N_P^L	$\rho_{\max}$ (%)	N_C	N_P^U
16	1.2	0.042	25 147	30.0	100	0.070	2.698	0.130	1.430	0.184	0.099
					200	0.063	1.908	0.165	1.320	0.261	0.129
					400	0.056	1.349	0.206	1.160	0.368	0.160
					800	0.050	0.954	0.262	0.980	0.521	0.191
					1600	0.046	0.675	0.344	0.820	0.737	0.227
					3200	0.042	0.477	0.440	0.654	1.042	0.256
30	2.4	0.065	31 008	30.0	100	0.123	1.867	0.165	2.240	0.311	0.139
					200	0.110	1.320	0.207	1.960	0.440	0.172
					400	0.099	0.933	0.265	1.650	0.622	0.205
					800	0.090	0.660	0.341	1.350	0.880	0.238
					1600	0.083	0.467	0.447	1.095	1.244	0.272
					3200	0.075	0.330	0.571	0.937	1.760	0.330
40	3.0	0.079	34 129	30.0	100	0.150	1.733	0.173	2.700	0.395	0.160
					200	0.135	1.225	0.220	2.270	0.559	0.190
					400	0.122	0.866	0.282	1.880	0.791	0.223
					800	0.111	0.613	0.362	1.550	1.118	0.260
					1600	0.102	0.433	0.471	1.300	1.581	0.308
					3200	0.100	0.306	0.653	1.106	2.236	0.0371
65	4.5	0.111	40 124	43.8	100	0.215	1.484	0.193	3.900	0.490	0.177
					200	0.194	1.050	0.246	3.260	0.693	0.209
					400	0.176	0.742	0.316	2.700	0.981	0.244
					800	0.162	0.525	0.412	2.290	1.387	0.293
					1600	0.146	0.371	0.526	1.940	1.961	0.351
					3200	0.132	0.262	0.672	1.600	2.774	0.410
76	5.0	0.124	42 271	49.1	100	0.237	1.448	0.196	4.400	0.528	0.183
					200	0.215	1.024	0.252	3.680	0.747	0.217
					400	0.195	0.724	0.323	3.000	1.056	0.250
					800	0.179	0.512	0.419	2.530	1.493	0.298
					1600	0.161	0.362	0.535	2.200	2.111	0.367
					3200	0.160	0.256	0.750	1.810	2.986	0.427

are the governing nondimensional numbers, $\tilde{M}$ is the nondimensional bending moment, and ϑ_n is the normalized local rotation. Eqs. (7) and (8) define the *stress* and the *reinforcement brittleness numbers*, introduced by Carpinteri [30,31]. As a result, each numerical simulation is completely described by a different couple of values s and N_P. In particular, the value of N_P relative to the condition of minimum reinforcement is referred to as N_P^L, where superscript L stands for "lower", since it will define the lower limit to the range of ductile response. The values of s and N_P^L for the numerical simulations carried out in this study are shown in Fig. 11(b) and reported in Table 1. In the range of interest for common structural applications, h ranging from 0.1 m up to 3.2 m, the trend obtained can be described with a very good approximation (goodness of fit $r^2 = 0.99$) by the following hyperbolic curve:

$$N_P^L = 0.26\, s^{-0.71}. \tag{9}$$

By substituting Eqs. (7) and (8) into (9), the following relationship between the minimum reinforcement percentage and the mechanical and geometrical properties of the beam is obtained:

$$\rho_{\min} = 0.26 \left(\frac{\sigma_u h^{0.5}}{K_{IC}}\right)^{0.71} \frac{K_{IC}}{\sigma_y h^{0.5}} = 0.26 \frac{\sigma_u^{0.71} K_{IC}^{0.29}}{\sigma_y h^{0.15}}. \tag{10}$$

The new proposed formula is compared to the prescriptions of the design codes in Fig. 12, where the values of minimum reinforcement are reported as functions of the beam height, h, for a concrete average compressive strength $\sigma_c = 40$ MPa, and a steel yielding strength $\sigma_y = 450$ MPa. In particular, $\rho_{\min}$ is defined as $A_{s,\min}/bh$, where $A_{s,\min}$ is the minimum reinforcement amount, in the hypothesis of a ratio between effective and overall depth, d/h, equal to 0.9. It can be seen that only the Norwegian Standards NS 3473 E (1989) account for the effect of the member size. On the contrary, all the other considered curves completely disregard the size-scale effects.

With respect to the proposed approach, a more complete study of the problem, for a definitive Standards improvement, should also consider the variability of the reinforcement cover,

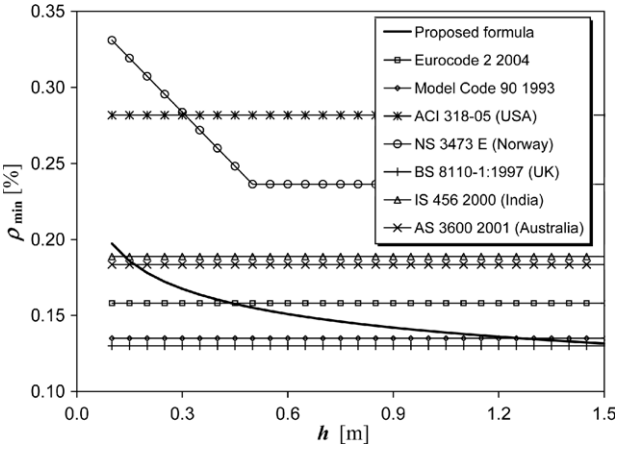

Fig. 12. Minimum reinforcement percentage, defined as $A_{s,\min}/bh$, vs. beam depth according to various design codes.

of the steel–concrete interface, as well as of the size and the number of the rebars. In this paper, it is assumed that they only marginally affect the brittle-to-ductile transition, that is the main investigated topic, together with the size effects. Furthermore, it is worth noting that more restrictive prescriptions for the minimum amount of reinforcement may arise from the limitations to the crack mouth opening displacement in the serviceability conditions, necessary to prevent steel corrosion and improve durability. Also in this case, size-effects are expected, as experimentally observed by Yasir Alam et al. [32]. In this context, the proposed model will permit to evaluate the crack mouth opening displacement under the serviceability loads by taking into account the closing contributions exerted by the cohesive forces along the fictitious crack. However, the interaction between cracks along the beam span and the steel–concrete interaction will play an important role in determining the correct value of the crack opening. The former effect can be considered by analysing a beam portion having a length equal to the crack spacing evaluated, for instance, according to the procedure proposed at the Par. 7.3.4. of the Eurocode 2 Part 1-1 [7]. Such a length, function of the bar diameter and the effective steel percentage, will influence the transfer length for the shear stresses between rebars and surrounding concrete and, therefore, the steel–concrete interaction. At this regards, more reliable results will be obtained by improving the algorithm with a step-by-step analysis of the bond–slip behaviour together with the crack propagation process.

4.2. Plastic rotation capacity

A second detailed numerical study is proposed to analyse the effect of each parameter to the plastic rotation capacity. With reference to the typical moment versus rotation curve obtained by the application of the proposed algorithm and shown in Fig. 13(a), the plastic component of the total rotation can be obtained as the difference between the rotation beyond which the moment starts descending rapidly and the rotation corresponding to the reinforcement yielding. It is worth noting that the softening or even snap-back branches at the end of the plastic plateau are usually due to concrete crushing, and can be captured only if the crushing zone extension is assumed to govern the loading process.

The results of several numerical simulations, carried out by considering different beam heights and reinforcement percentages, are summarized in the plastic rotation, ϑ_{PL}, vs. relative neutral axis position, x/d, diagram shown in Fig. 13(b). Such a diagram is consistent with the practical prescriptions of the Eurocode 2 [7], of whom, that relative to high ductility steel and concrete compressive strength less than or equal to 50 MPa is also provided (dashed curve in Fig. 13(b)). Beams with a height equal to 0.2 m have a rotational capacity greater than that suggested by the code. On the other hand, by increasing the beam height up to 0.8 m, the rotations provided by the code appear to be not conservative. It is worth noting that the numerical results for $h = 0.4$ m are in good agreement with the curve provided by the code, which represents the 5%-fractile of the plastic rotations of beams or slabs with height of about 0.3 m (see [33] for more details). The new proposed curves can be easily used in structural design. In the case of a plastic structural analysis, in fact, the designer has to verify that the rotation required for the moment redistribution is lower than the admissible one. To this aim, for a given value of x/d obtained from the application of the ultimate state analysis, he can enter Fig. 13(b) and determine the admissible plastic rotation as a function of the beam size.

It is evident from the diagrams in Fig. 13(b) that the plastic rotation capacity tends to zero as the neutral axis relative position coordinate increases, i.e. the tensile reinforcement percentage increases. In particular, it is possible to define an upper limit to the reinforcement amount beyond which the steel does not yield, and the beam collapses in compression, without the development of a significant ductility. Such a limit, function of all the variables involved in the phenomenon, can be obtained by means of dimensional analysis, as previously done for the minimum reinforcement. Since now we are interested in over-reinforced concrete beams, the Buckingham's Π-Theorem is applied to the general functional relationship expressed in Eq. (4) by omitting the parameters describing the behaviour of concrete in tension, σ_u and $\mathcal{G}_F$. When h and $\sqrt{\mathcal{G}_C E_c}$ are assumed as the dimensionally independent variables, the dimensionless functional relationship becomes:

$$\tilde{M} = \Phi_2(N_C, N_P, \vartheta_n), \tag{11}$$

where:

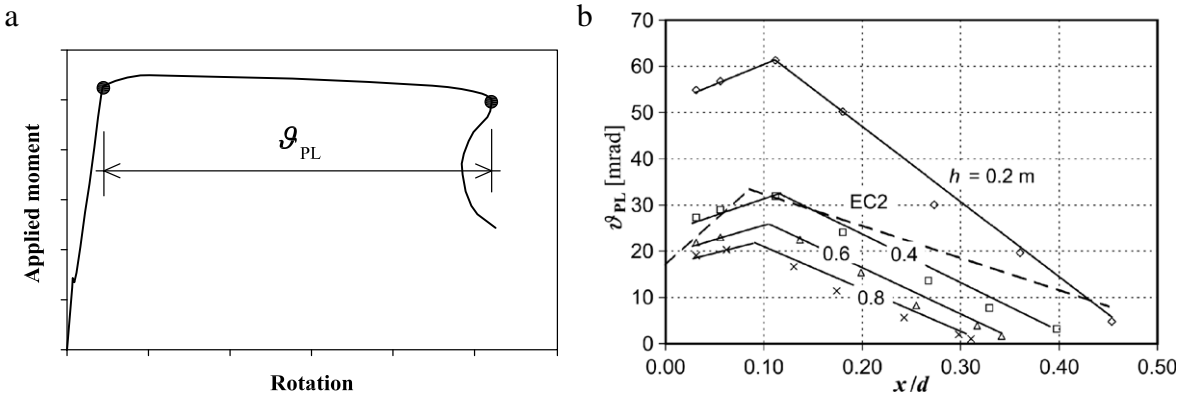

Fig. 13. Definition of plastic rotation (a); and predicted plastic rotation for different beam heights (solid lines) compared with the Eurocode 2 prescription (dashed line) (b).

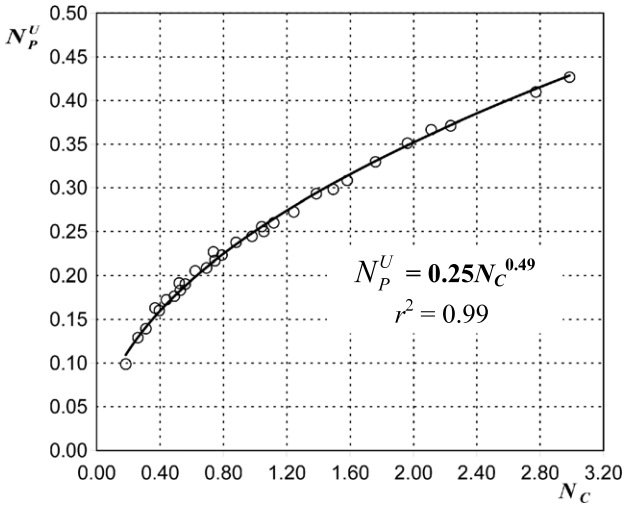

Fig. 14. Best-fit relationship of numerical results (not filled-in symbols) between N_P^U and N_C.

$$\tilde{M} = \frac{M}{h^{2.5}\sqrt{\mathcal{G}_C E_c}}, \tag{12}$$

$$\vartheta_n = \vartheta \frac{E_c h^{0.5}}{\sqrt{\mathcal{G}_C E_c}}, \tag{13}$$

$$N_P = \rho \frac{\sigma_y h^{0.5}}{\sqrt{\mathcal{G}_C E_c}} \tag{14}$$

and

$$N_C = \frac{\sigma_c h^{0.5}}{\sqrt{\mathcal{G}_C E_c}}. \tag{15}$$

N_P and N_C are two nondimensional numbers defined for over-reinforced concrete beams.

The beams considered in the previous section for the evaluation of the minimum reinforcement are now analysed in case of high reinforcement amount. In particular, for each of the beams, several numerical simulations have been carried out in order to find the limit value of the reinforcement percentage beyond which the steel does not yield. The values of N_P corresponding to this situation, referred to as N_P^U, where superscript U stands for "upper" limit, are reported together with the values of N_C in Table 1. In the considered range for the beam height, the relationship between N_P^U and N_C can be described with a very good approximation (goodness of fit $r^2 = 0.99$) by the following power law (see Fig. 14):

$$N_P^U = 0.25 N_C^{0.49}. \tag{16}$$

By substituting Eqs. (14) and (15) into (16), the maximum reinforcement can be expressed as a function of the mechanical and geometrical properties, as follows:

$$\rho_{\max} = 0.25 \frac{\sigma_c^{0.49} \left(\sqrt{\mathcal{G}_C E_c}\right)^{0.51}}{\sigma_y h^{0.25}}. \tag{17}$$

5. Discussion and conclusions

In the present paper, a numerical method able to describe the nonlinear behaviour of RC members during both tensile fracturing and compression crushing has been presented. With the proposed algorithm, based on nonlinear fracture mechanics concepts, it is possible to completely capture the moment vs. rotation response of all the intermediate situations ranging from plain concrete to over-reinforced concrete beams under monotonic loadings. In particular, the problem of minimum reinforcement and the behaviour of plastic hinges have been analysed in order to highlight the limits of the code prescriptions and provide new easy-to-use design formulae and diagrams.

According to the new proposal expressed by Eq. (10), the minimum reinforcement percentage, $\rho_{\min}$, is an increasing function of the concrete tensile strength and toughness, whereas it decreases as the steel yielding strength and the beam height increase. As regards the size-scale effects, the presence of cohesive closing stresses determines a variation in $\rho_{\min}$ with the beam size described by the power $h^{-0.15}$. With reference to the existing code provisions, the proposed formula permits to save steel reinforcement in the case of large structures.

As far as the plastic rotation capacity is concerned, the numerical results obtained, summarized in Fig. 13(b), show that ϑ_{PL} is not only dependent on the neutral axis position. This assumption, in fact, leads to over-estimate the rotational capacity of deep beams. In order to improve the code provisions, the effect of the structural dimension should be explicitly taken into account by considering different design curves as, for instance, those proposed in Fig. 13(b).

As a result of the comprehensive investigation proposed in this paper, the conditions for the structural design of RC elements exhibiting ductile response can be highlighted. From a qualitative point of view, the decrease in one parameter among h, ρ, and σ_y, or the increase in σ_u or $\mathcal{G}_F$, all the other parameters being kept constant, determines a transition from ductile response to unstable tensile crack propagation, as represented in Fig. 15(a). On the other hand, the increase in h, or ρ, or σ_y, or the decrease in σ_c or $\mathcal{G}_C$, all the other parameters being kept constant, produces a transition towards crushing failure without steel yielding (see

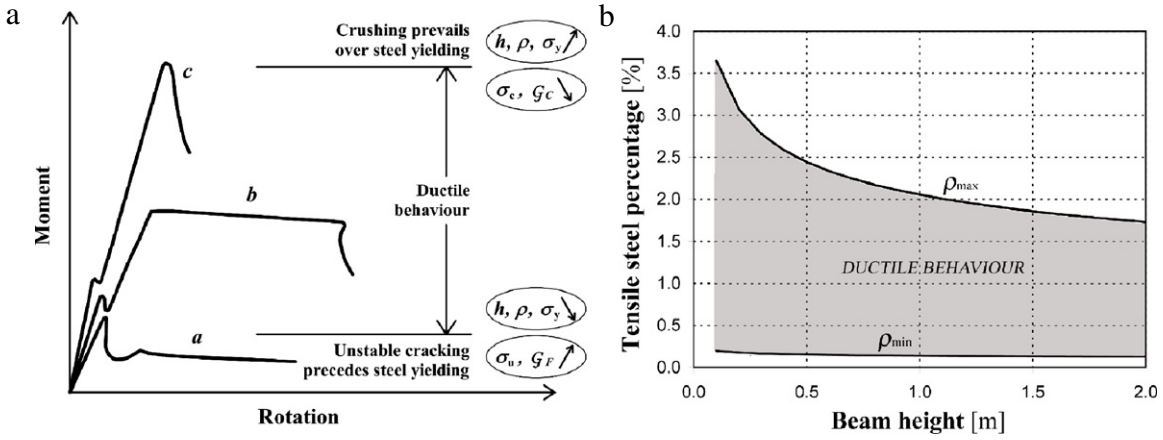

Fig. 15. Conditions for structural design of RC members with ductile response (a); and corresponding limit values for the tensile steel reinforcement (b).

Fig. 15(a)). The exact values of the upper and the lower bounds to the reinforcement percentage given by Eqs. (10) and (17) are shown in Fig. 15(b) as a function of the beam height, for an average concrete compressive strength $\sigma_c = 40$ MPa, and a steel yield strength $\sigma_y = 450$ MPa.

Finally, although the proposed approach has been proved to be very effective in the situations characterized by a high gradient in the bending moment diagram, such as in the three-point-bending problem or in the portion over an intermediate support of a continuous beam, it can be profitably apply also to a more general frame calculation. The moment vs. rotation relationships representative of the behaviour of the plastic hinge regions, in fact, can be adopted in a step-by-step plastic structural analysis, replacing the usually used elasto-perfectly plastic law without limitation to the maximum rotation. In this case, the bending moment redistribution, and, therefore, the ultimate load carrying capacity, could be determined by the achievement of the size-dependent rotational capacity in one of the plastic hinges, before the formation of a perfectly-plastic collapse mechanism.

Acknowledgements

The financial supports provided by the Ministry of University and Scientific Research (MIUR) to the project "Advanced applications of Fracture Mechanics for the study of integrity and durability of materials and structures", and by the Regione Piemonte to the RE-FRESCOS project "Preservation, safeguard and valorization of masonry decorations in the architectural historical heritage of Piedmont", are gratefully acknowledged.

References

[1] von Kármán T, Tsien HS. The buckling of thin cylindrical shells under axial compression. J Aerosol Sci 1941;8:303–12.
[2] Carlson RL, Sendlebeck RL, Hoff NJ. Experimental studies of the buckling of complete spherical shells. Exp Mech 1967;7:281–8.
[3] Kaplan A. Buckling of spherical shells. In: Fung YC, Sechler EE, editors. Thin shell structures, theory, experiment, and design. Englewood Cliffs (NJ): Prentice-Hall Inc.; 1974. p. 248–88.
[4] Carpinteri A. Interpretation of the Griffith instability as a bifurcation of the global equilibrium. In: Shah SP, editor. Proc. NATO advanced research workshop on application of fracture mechanics to cementitious composites. Dordrecht (The Netherlands): Martinus Nijhoff Publishers; 1985. p. 287–316.
[5] Carpinteri A. Size effects on strength, toughness, and ductility. J Eng Mech, ASCE 1989;115:1375–92.
[6] Comité Euro-International du Béton. CEB-FIP model code 1990. Lausanne: Thomas Telford Ltd.; 1993.
[7] CEN TC/250. Eurocode 2: design of concrete structures, part 1–1: general rules and rules for buildings. Brussels. 2004.
[8] van Mier JGM. Strain-softening of concrete under multiaxial loading conditions. Ph.D. thesis. Eindhoven University of Technology. 1984.
[9] Jansen DC, Shah SP. Effect of length on compressive strain softening of concrete. J Eng Mech 1997;123:25–35.
[10] Carpinteri A, Corrado M, Mancini G, Paggi M. The overlapping crack model for uniaxial and eccentric concrete compression tests. Mag Concr Res 2009;61:745–57.
[11] Carpinteri A, Corrado M, Paggi M. An analytical model based on strain localization for the study of size-scale and slenderness effects in uniaxial compression tests. Strain 2011;47:351–62.
[12] Zhu W, Bartos PJM. Effects of combined fiber treatments and matrix modifications on toughness of aged GRC. In: Proc. of the 9th congress of the GRCA. 1993. p. 4/I–IX.
[13] Bosco C, Carpinteri A, Debernardi PG. Minimum reinforcement in high-strength concrete. J Struct Eng, ASCE 1990;116:427–37.
[14] Jenkins MG, Kobayashi AS, White KW, Bradt RC. Crack initiation and arrest in a sic whisker/AL2O3 matrix composite. J Am Ceram Soc 1987;70:393–5.
[15] Carpinteri A. A fracture mechanics model for reinforced concrete collapse. In: Proc., IABSE colloquium, delft. The Netherlands: Delft University Press; 1981. p. 17–30.
[16] Bosco C, Carpinteri A. Softening and snap-through behavior of reinforced elements. J Eng Mech 1992;118:1564–77.
[17] Carpinteri A, Massabò R. Bridged versus cohesive crack in the flexural behaviour of brittle-matrix composites. Int J Fract 1996;81:125–45.
[18] Corley GW. Rotational capacity of reinforced concrete beams. J Struct Div 1966;92:121–46.
[19] Bigaj AJ, Walraven JC. Size effect on rotational capacity of plastic hinges in reinforced concrete beams. CEB Bull Inf 1993;218:7–23.
[20] Bosco C, Debernardi PG. Influence of some basic parameters on the plastic rotation of reinforced concrete elements. CEB Bull Inf 1993;218:25–44.
[21] Carpinteri A, Corrado M, Paggi M, Mancini G. Cohesive versus overlapping crack model for a size effect analysis of RC elements in bending. Carpinteri A, Gambarova P, Ferro G, Plizzari G, editors. Proc. of the 6th int. FraMCoS conference, vol. 2. Leiden (The Netherlands): Taylor & Francis; 2007. p. 655–63.
[22] Carpinteri A, Corrado M, Paggi M. An integrated cohesive/overlapping crack model for the analysis of flexural cracking and crushing in RC beams. Int J Fract 2010;161:161–73.
[23] Hillerborg A, Modeer M, Petersson PE. Analysis of crack formation and crack growth in concrete by means of fracture mechanics and finite elements. Cem Concr Res 1976;6:773–82.
[24] Kotsovos MD. Effect of testing techniques on the post-ultimate behaviour of concrete in compression. RILEM Mater Struct 1983;16:3–12.
[25] Hillerborg A. Fracture mechanics concepts applied to moment capacity and rotational capacity of reinforced concrete beams. Eng Fract Mech 1990;35:233–40.
[26] Carpinteri A, Corrado M. An extended (fractal) overlapping crack model to describe crushing size-scale effects in compression. Eng Fail Anal 2009;16:2530–40.
[27] Suzuki M, Akiyama M, Matsuzaki H, Dang TH. Concentric loading test of RC columns with normal- and high-strength materials and averaged stress–strain model for confined concrete considering compressive fracture energy. In: Proc. 2nd fib congress. 2006.
[28] Ruiz G, Elices M, Planas J. Size effects and bond–slip dependence of lightly reinforced concrete beams. In: Carpinteri A, editor. Minimum reinforcement in concrete members. Oxford (UK): Elsevier Science Ltd.; 1999. p. 127–80.
[29] Buckingham E. Model experiments and the form of empirical equations. ASME Trans 1915;37:263–96.
[30] Carpinteri A. Static and energetic fracture parameters for rocks and concretes. RILEM Mater Struct 1981;14:151–62.
[31] Carpinteri A. Stability of fracturing process in RC beams. J Struct Eng, ASCE 1984;110:544–58.
[32] Yasir Alam S, Lenormand T, Loukili A, Regoin JP. Measuring crack width and spacing in reinforced concrete members. In: Oh BH, editor. Proc. of the 7th int. FraMCoS conference. Seoul (Korea): Korea Concrete Institute; 2010. p. 377–82.
[33] Eligehausen R, Fabritius E, Li L, Zhao R. An analysis of rotation capacity tests. CEB Bull Inf 1993;218:251–73.